Shock Waves in Weakly Compressed Granular Media

Siet van den Wildenberg, Rogier van Loo, and Martin van Hecke
Kamerling Onnes Lab, Universiteit Leiden, Postbus 9504, 2300 RA Leiden, The Netherlands
(Received 25 April 2013; published 22 November 2013)

We experimentally probe nonlinear wave propagation in weakly compressed granular media and observe a crossover from quasilinear sound waves at low impact to shock waves at high impact. We show that this crossover impact grows with the confining pressure P_0, whereas the shock wave speed is independent of P_0—two hallmarks of granular shocks predicted recently. The shocks exhibit surprising power law attenuation, which we model with a logarithmic law implying that shock dissipation is weak and qualitatively different from other granular dissipation mechanisms. We show that elastic and potential energy balance in the leading part of the shocks.

DOI: 10.1103/PhysRevLett.111.218003 PACS numbers: 45.70.−n, 81.05.Rm

Many disordered materials, including granular media [1–4], foams [5], and emulsions [6,7], lose their rigidity when their confining pressure P_0 is lowered. In almost all cases, the resulting unjamming transition goes hand in hand with the vanishing of one or both elastic moduli [8–17], and consequently, nonlinearities must dominate when such marginal systems are subjected to finite stresses [1,18,19]. For example, soft particles exhibit nonlinear rheology near jamming [6,20], even when their local elastic and viscous interactions are linear [21,22], and marginally connected spring networks exhibit nonlinear elasticity near their critical points [23,24]. In these two cases, the vanishing of the elastic moduli is a collective phenomenon, closely connected to the isostatic character of the marginal state [8–17].

Here, we experimentally probe a different scenario where local nonlinearities near unjamming lead to vanishing elastic moduli and nonlinear excitations: shock waves in granular media [25]. Granular media have frictional interactions, and frictional media in general do not reach the isostatic limit: there are thus no collective mechanisms leading to vanishing elastic moduli or nonlinearities [15,26–28]. Nevertheless, when granular media unjam as the pressure P_0 is lowered, the individual contacts weaken due to the nonlinear local Hertz contact law, which states that for elastic spheres, the contact forces f scale with deformations δ as $f \sim \delta^{3/2}$ [29,30]. As a result, frictional granular media have a vanishing linear response at their unjamming point, and their elastic moduli and sound speed vanish as $P_0^{1/3}$ and $P_0^{1/6}$, respectively [10,31–34].

Recent simulations on frictionless Hertzian media by Gomez *et al.* suggest that sound waves give way to strongly nonlinear shock waves near the unjamming ($P_0 \to 0$) point [1]. Three crucial questions remain open, as the numerical model of Gomez has no static friction, no dissipation, and is in 2D. First, realistic granular media are frictional: do shock waves also arise for nonisostatic, frictional systems? Second, friction also leads to dissipation—do shock waves survive realistic levels of dissipation? Third, can such shock waves be excited in 3D experiments?

To answer these questions, we experimentally probe sound and shock waves by impacting a weakly compressed granular medium with a heavy mass, while measuring the propagation speed and front shape for a wide range of impact magnitudes (Fig. 1). We find that we excite shock waves, which exhibit the three main hallmarks of the numerically observed conservative shocks: (i) a crossover from linear waves to shock waves when the impact pressure P exceeds the confining pressure P_0; (ii) independence of the shock speed on P_0 but power law scaling with impact strength; (iii) a balance of kinetic and potential energies in the leading edge of the shock waves.

Moreover, we find a novel power law attenuation of the shock waves, which we can capture by a simple model where the local dissipation depends logarithmically on grain forces—this dissipation is qualitatively different from other granular dissipation mechanisms. The ease with which we can excite such granular shock waves

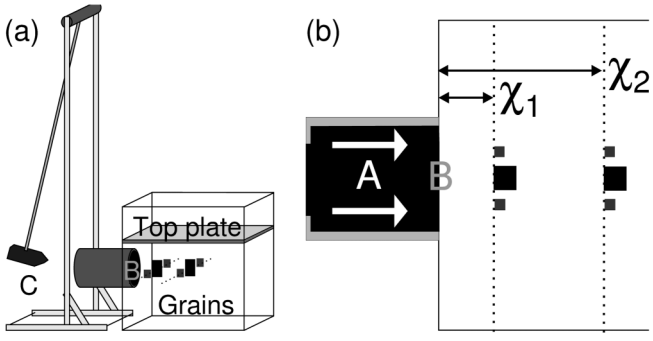

FIG. 1. Schematic side view (a) and top view (b) of our setup. Shock waves are excited in the granular medium by a plunger (A) which slides through a circular hole (B) and is impacted by a heavy mass (C). Pressure sensors and accelerometers (big, respectively, small squares—both enlarged for visibility) are attached to steel wires immersed in the granular medium at locations χ_1 and χ_2.

suggests that they play an important role whenever loose granular media are strongly excited [35–39].

Setup.—Our setup consists of a large metal container ($45 \times 45 \times 45$ cm) filled with glass beads (diameter $D = 3.8$–4.4 mm) and covered by a 2 kg aluminum top plate. To excite shock waves, we impact a freely sliding cylindrical piston (A), (diameter 10 cm, length 18 cm, mass 3.7 kg), which makes contact with the grains through a circular hole in the side of the container (B), with a mass (C, 1.2 kg) suspended from a pendulum (mass 2 kg, length 1.3 m). We detect wave propagation throughout the material via pressure sensors and accelerometers buried in the granular medium; the sensors are attached to steel wires to ensure their correct positioning and orientation. We thus probe the local excess pressure (our pressure sensors have no dc response) and acceleration at distances χ_1 and χ_2 from the impact zone (Fig. 1).

Phenomenology.—In Fig. 2, we show typical time traces of the local pressures and velocities detected at locations $\chi_1 = 5$ cm and $\chi_2 = 15$ cm, for a strong impact and low confining pressure. The waves take the form of fronts with a clearly identifiable leading edge, where the pressures and particle velocities peak, followed by a long tail with a complex structure. We characterize our waves by the peak pressures, P_{χ_1} and P_{χ_2}, and peak particle velocities, u_1 and u_2, at χ_1 and χ_2. We determine the front speed V_s from the time of travel Δt, where Δt is the interval between P reaching its 50% value at χ_1 and χ_2.

From data such as presented in Fig. 2, we can deduce that elastic deformations dominate the physics of the leading edge of the shock, by connecting the force per particle and its displacement through Hertz law. The peak force per particle χ_1 can be estimated using the contact area of the pressure sensor (1.33 cm^2) to be of order 0.6 N. Typical contact deformations then follow from Hertz law, which relates the contact force F and deformation δ as $F = \frac{4}{3}E^* R^{1/2}\delta^{3/2}$ [29]. Taking $E^* = 50$ GPa (typical value for glass), we estimate that $\delta \approx 0.35$ μm. The location χ_1 is 12 particle diameters ≈ 24 contact zones away, so the cumulative motion x at χ_1 is predicted to be of order 8 μm. Integrating the velocity signal [Fig. 2(c)] up to its peak at time $t^* \approx 0.13$ ms, we estimate the displacement at t^* to be also 8 μm. This suggests that in the leading edge of the wave, the deformations are predominantly elastic.

The picture that emerges is that upon impact, a rapid front is formed, which, for the cases when V_s is larger than the sound speed, we will call a shock wave. We note that while the grain displacements at $t = t^*$ are of the order of μm's, the total motion of the plunger into the sand is of the order of a mm: long after the shock wave has outrun our system, the plunger is still slowly penetrating the sand bed, leading to a very long tail, where the vast majority of rearrangements and dissipative events take place [33,34].

Propagation speed.—To probe the nature of the waves excited in this system, we varied the pressure P_0 at the depth of the sensors from 0.9 to 6 kPa and determined the propagation speed V_s for a wide range of impact strengths. To compare our data to the theoretical predictions of [1], we plot our data in a so-called Hugoniot plot. Due to attenuation (see Fig. 2), $P_{\chi_2} < P_{\chi_1}$ and we therefore use their geometric mean, $P_m := \sqrt{P_{\chi_1} P_{\chi_2}}$, as a measure of the impact strength.

Figure 3 shows V_s as a function of P_m and P_0, and our data are well fit by the form $V_s = C(1 + P_m/P_f)^{1/6}$, which is a phenomenological fit capturing the plateau at low impacts and power law at large impacts. We note that the exact result for the 2D frictionless shocks, as given by Eq. 5 of [1], is similar to this fit.

The main three features are the following. (i) For strong impacts, V_s becomes independent of P_0, and V_s scales

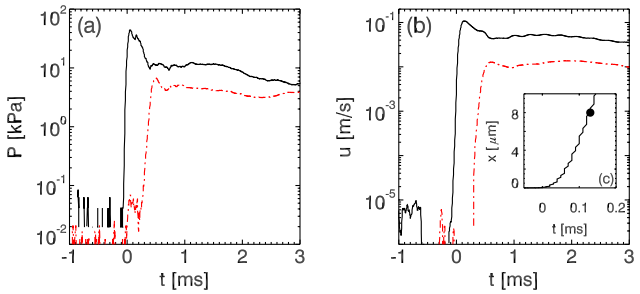

FIG. 2 (color online). Typical signals for high impact amplitude, for $P_0 = 0.9$ kPa, at $\chi_1 = 5$ cm (black) and $\chi_2 = 15$ cm (red, dashed). (a) Local pressures $P(t)$. (b) Local velocities $u(t)$ obtained by integrating the acceleration signal. (c) Local displacement obtained by integrating the velocity signal. The dot represents the cumulative displacement at the peak velocity.

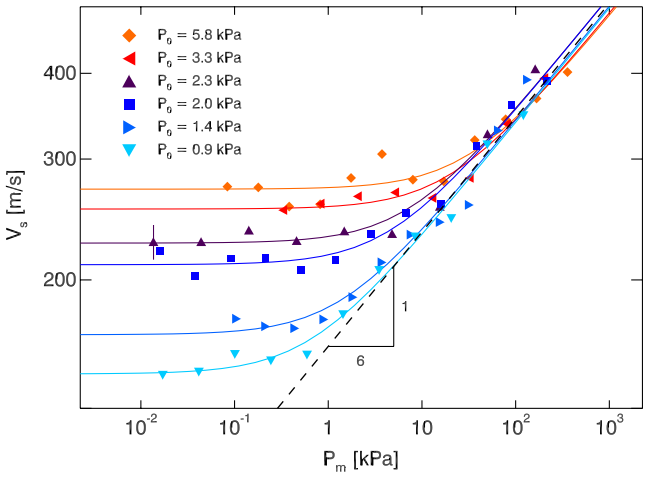

FIG. 3 (color online). Front speed v_s as a function of peak pressure in the front, P_m, for a range of confining pressures P_0, at $\chi_1 = 5$ cm at $\chi_2 = 15$ cm. Each data point corresponds to a number of runs, and we indicated a typical 5% error bar. Fits (solid lines) are functions of the form $V_s = C(1 + P_m/P_f)^{1/6}$. For $P_m \gg P_0$, $V_s \sim P_m^{1/6}$ (dashed line) and is independent of P_0.

consistently as $P_m^{1/6}$—the dependence on P_m is a hallmark of nonlinear waves, and the exponent $1/6$ is the one predicted for Hertzian shock waves. (ii) For weak impacts, V_s becomes independent of the impact strength—the hallmark of linear waves—but increases with pressure due to the nonlinear local interaction law. (iii) The crossover from the linear to nonlinear regime is expected to arise when $P_m \gg P_0$, because when $P_m \gg P_0$, linearization fails [1]. Indeed, we find that P_f grows with P_0.

All these features are in good qualitative and quantitative agreement with the earlier numerical findings of Gomez *et al.*: the waves we excite for large impacts are indeed shock waves.

Attenuation.—The peak pressure diminishes whilst the shock propagates through the material. In Fig. 4, we compare the peak pressures P_{χ_1} and P_{χ_2} at $\chi_1 = 5$ cm and $\chi_2 = 15$ cm for the same experiments as shown in Hugoniot plot. Strikingly, the attenuation varies significantly with impact strength: for the weakest impacts, $P_{\chi_2} \approx P_{\chi_1}$, while for larger impacts the relation between P_{χ_2} and P_{χ_1} is consistent with power law scaling:

$$\text{For } \tilde{P} \geq 1\text{: } \tilde{P}_2 = \tilde{P}_1^{\beta}, \tag{1}$$

$$\text{For } \tilde{P} \leq 1\text{: } \tilde{P}_2 = \tilde{P}_1, \tag{2}$$

where $\tilde{P} := P/P^*$, $\tilde{P}_{1,2} := P_{\chi_{1,2}}/P^*$, the characteristic pressure $P^* \approx 50$ Pa and $\beta \approx 0.77 \pm 0.05$.

We will now determine a simple local model that captures this remarkable power law attenuation. We ignore disorder and imagine the signal to propagate over a linear chain of beads, where each bead attenuates the signal by a factor $(1 - \varepsilon)$. We assume the local attenuation ε to depend on the local pressure P only:

$$P^{i+1} = [1 - \varepsilon(P^i)]P^i. \tag{3}$$

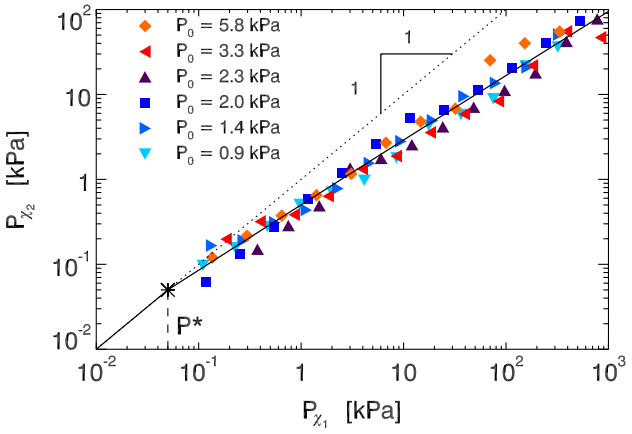

FIG. 4 (color online). Scatter plot of the maximum pressures P_{χ_1} and P_{χ_2} at $\chi_1 = 5$ cm and $\chi_2 = 15$ cm for a range of pressures—same data as in Fig. 3. The black curve is a fit to our model given by Eqs. (3)–(6).

Taking the continuum limit yields:

$$\frac{dP}{dx} = -\frac{\varepsilon(P)}{D}P. \tag{4}$$

One can easily show [40] that we can capture the power law relation between P_{χ_1} and P_{χ_2} when $\varepsilon(P)$ has the following logarithmic form [Fig. 5(a)]:

$$\text{For } P \geq P^*\text{: } \varepsilon(P) = \varepsilon_s \ln\left(\frac{P}{P^*}\right), \tag{5}$$

$$\text{For } P \leq P^*\text{: } \varepsilon(P) = 0, \tag{6}$$

where $\varepsilon_s := -\ln(\beta)D/(\chi_2 - \chi_1)$ is a material constant.

A surprising consequence of this model is that it predicts that the exponent β should depend on the distance between χ_2 and χ_1. To test this, we have performed several sets of experiments where we vary this distance. Figure 5(b) shows that the log slope relating P_{χ_1} and P_{χ_2} indeed increases for larger propagation distance between χ_2 and χ_1. These trends are captured by our model, for a single value of $\varepsilon_s = 3.46$, and without any additional fit parameters.

Local Elastic Motion and Energy Balance.— Figure 5(a) illustrates that even for the strongest impacts, the attenuation per particle is less than 10%. This motivates us to probe the balance between elastic and potential energies in our shock waves. For the conservative shocks studied in the numerical simulations [1], the kinetic and potential energies balance in the shock regime, whereas away from the shock regime, the kinetic energy tends to zero, but the potential energy saturates at its lower bound $\sim P_0^{5/3}$.

To probe this balance in our experimental data, we present scatter plots of the peak velocities u_1 and u_2 vs the peak pressures P_{χ_1} and P_{χ_2} in Fig. 6. The kinetic energy simply scales $\sim u_m^2$, where u_m is the maximum local velocity, whereas the potential energy for Hertzian contacts scales $\sim \delta_m^{5/2} \sim f_m^{5/3}$, where δ_m and f_m are the local maximum deformations and forces. Note that the contact force f_m should contain both the dc component $\propto P_0$ and ac component $\propto P_{\chi_{1,2}}$. Our data are fully consistent with a $5/6$ power law in the strongly nonlinear regime, and a pressure dependent deviation from this law in the weakly nonlinear

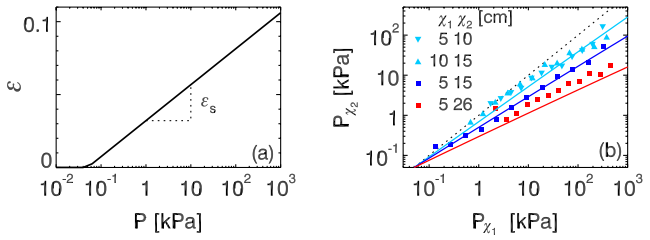

FIG. 5 (color online). (a) Attenuation per contact $\varepsilon(P)$. (b) Scatter plot of P_1 and P_2 for $P_0 = 1.4$ kPa at various locations χ_1 and χ_2, and corresponding fits to our model.

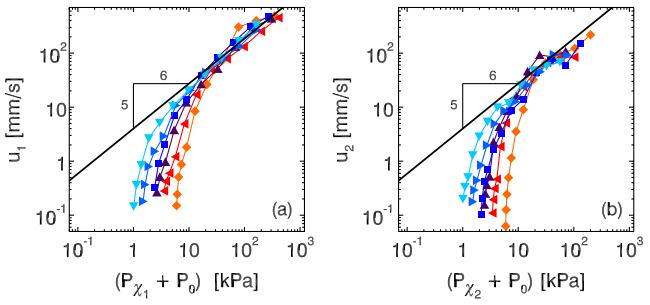

FIG. 6 (color online). A comparison of the peak velocities and peak pressures at (a) $\chi_1 = 5$ cm and (b) $\chi_2 = 15$ cm.

regime, and shows a strikingly good qualitative agreement with the numerical data by Gomez *et al.* [Fig. 3(d) of [1]]. We finally note that this balance is equally good at χ_1 and χ_2, even though the energies in χ_2 are smaller than in χ_1 due to attenuation. All this suggest that the attenuation does not significantly upset the balance between kinetic and potential energies.

Discussion.—By varying the impact strength, we can tune our waves from pressure dependent sound waves at low impact, to pressure independent nonlinear shock waves at higher impact, similar to what was predicted for dissipationless Hertzian particles [1]. We find that propagating from one grain to the next, a small amount of energy is dissipated, which leads to novel power law scaling of the attenuation of the shocks amplitude over several decades. Is this attenuation caused by scattering or dissipation? While we cannot rule out scattering, we note that the overall decrease of the pressure and velocity profiles shown in Fig. 2 favors a dissipative picture; in addition, the width of the leading edge does not change very much under propagation. Notwithstanding this weak dissipation, the magnitude of displacements in the shock, and the balance of kinetic and potential energy, show that the physics in the leading edge of the shock is dominated by elastic interactions.

The shock waves we observe here are therefore qualitatively different from the slow granular densification waves known as "plowing" [35,41]. Plowing is associated with densification through highly dissipative rearrangements, and such densification fronts propagate with velocities far below the sound speed [35]. Similarly slow and dissipative events may occur in the tail of our waves, but the point is that the leading edge of our shock waves propagates faster than the sound speed. These shock waves are also qualitatively different from the weakly nonlinear waves observed under continuous driving [33,34].

We stress here that the log type of dissipation observed is very different from ordinary granular dissipation. For example, linear wave attenuation is typically associated with a constant value of ϵ, leading to exponential attenuation in space and a linear relation between P_{χ_1} and P_{χ_2}. Dissipation based on inelastic collisions takes a power law form [42–44]—however, the relation between P_{χ_2} and P_{χ_1} is not itself a power law for power law dissipation [45]. We are not aware of any other examples where one finds a similar nontrivial power law relation between P_{χ_1} and P_{χ_2}, which may be a unique feature of shock waves. We note that this form of dissipation leads to two new characteristic scales, $P^* \approx 50$ Pa and $\varepsilon_s \approx 3.5$, not present in the frictionless problem.

Finally, we note the relevance of the relative magnitude of the two characteristic pressure scales—the external pressure P_0 that sets the crossover from linear to shock waves, and the characteristic pressure P^* above which attenuation sets in. In our experiment, $P_0 \gg P^*$, but it is conceivable that for more elastic particles, or in microgravity, one can reach $P_0 \ll P^*$, in which case, virtually dissipation free granular shock waves could be observed.

We acknowledge discussions with J. Burton, L. Gomez, H. Jaeger, X. Jia, and V. Vitelli. This work is part of the Industrial Partnership Programme (IPP) Innovative Physics for Oil and Gas (iPOG) of the Stichting voor Fundamenteel Onderzoek der Materie (FOM), which is supported financially by Nederlandse Organisatie voor Wetenschappelijk Onderzoek (NWO). The IPP iPOG is cofinanced by Stichting Shell Research.

[1] L. R. Gomez, A. M. Turner, M. van Hecke, and V. Vitelli, Phys. Rev. Lett. **108**, 058001 (2012).
[2] T. S. Majmudar, M. Sperl, S. Luding, and R. P. Behringer, Phys. Rev. Lett. **98**, 058001 (2007).
[3] X. Cheng, Phys. Rev. E **81**, 031301 (2010).
[4] D. Bi, J. Zhang, B. Chakraborty, and R. P. Behringer, Nature (London) **480**, 355 (2011).
[5] G. Katgert and M. van Hecke, Europhys. Lett. **92**, 34002 (2010).
[6] K. N. Nordstrom, E. Verneuil, P. E. Arratia, A. Basu, Z. Zhang, A. G. Yodh, J. P. Gollub, and D. J. Durian, Phys. Rev. Lett. **105**, 175701 (2010).
[7] I. Jorjadze, L. L. Pontani, and J. Brujic, Phys. Rev. Lett. **110**, 048302 (2013).
[8] F. Bolton and D. Weaire, Phys. Rev. Lett. **65**, 3449 (1990).
[9] D. J. Durian, Phys. Rev. Lett. **75**, 4780 (1995).
[10] H. A. Makse, N. Gland, D. L. Johnson, and L. M. Schwartz, Phys. Rev. Lett. **83**, 5070 (1999); D. L. Johnson, H. A Makse, N. Gland, and L. Schwartz, Physica (Amsterdam) **279B**, 134 (2000); H. A. Makse, N. Gland, D. L. Johnson, and L. Schwartz, Phys. Rev. E **70**, 061302 (2004).
[11] C. S. O'Hern, L. E. Silbert, A. J. Liu, and S. R. Nagel, Phys. Rev. E **68**, 011306 (2003).
[12] W. G. Ellenbroek, E. Somfai, M. van Hecke, and W. van Saarloos, Phys. Rev. Lett. **97**, 258001 (2006).
[13] S. Dagois-Bohy, B. P. Tighe, J. Simon, S. Henkes, and M. van Hecke, Phys. Rev. Lett. **109**, 095703 (2012).
[14] C. P. Goodrich, A. J. Liu, and S. R. Nagel, Phys. Rev. Lett. **109**, 095704 (2012).

[15] M. van Hecke, J. Phys. Condens. Matter **22**, 033101 (2010).

[16] A. J. Liu and S. R. Nagel, Annu. Rev. Condens. Matter Phys. **1**, 347 (2010).

[17] The only counterexample of a system retaining finite elastic moduli near jamming we know of are frictional harmonic particles, which are not isostatic [15].

[18] V. Vitelli and M. van Hecke, Nature (London) **480**, 325 (2011).

[19] C. F. Schreck, T. Bertrand, C. S. O'Hern, and M. D. Shattuck, Phys. Rev. Lett. **107**, 078301 (2011).

[20] G. Katgert, M. E. Möbius, and M. van Hecke, Phys. Rev. Lett. **101**, 058301 (2008); G. Katgert, A. Latka, M. E. Möbius, and M. van Hecke, Phys. Rev. E **79**, 066318 (2009).

[21] P. Olsson and S. Teitel, Phys. Rev. Lett. **99**, 178001 (2007).

[22] B. P. Tighe, E. Woldhuis, J. J. C. Remmers, W. van Saarloos, and M. van Hecke, Phys. Rev. Lett. **105**, 088303 (2010).

[23] M. Wyart, H. Liang, A. Kabla, and L. Mahadevan, Phys. Rev. Lett. **101**, 215501 (2008).

[24] C. P. Broedersz, X. Mao, T. C. Lubensky, and F. C. MacKintosh, Nat. Phys. **7**, 983 (2011).

[25] We use the term shock waves here in a loose sense, meaning strongly nonlinear waves.

[26] E. Somfai, M. van Hecke, W. G. Ellenbroek, K. Shundyak, and W. van Saarloos, Phys. Rev. E **75**, 020301 (2007).

[27] K. Shundyak, M. van Hecke, and W. van Saarloos, Phys. Rev. E **75**, 010301 (2007).

[28] S. Henkes, M. van Hecke, and W. van Saarloos, Europhys. Lett. **90**, 14003 (2010).

[29] K. L. Johnson, *Contact Mechanics* (Cambridge University Press, Cambridge, England, 1987).

[30] For purely 2D Hertzian contacts, $f \sim \delta^{\alpha}$ with $\alpha = 1$, although 2D discs in experiments have somewhat larger exponents α [2].

[31] E. Somfai, J.-N. Roux, J. H. Snoeijer, M. van Hecke, and W. van Saarloos, Phys. Rev. E **72**, 021301 (2005).

[32] V. F. Nesterenko, J. Appl. Mech. Tech. Phys. **24**, 733 (1984); V. F. Nesterenko, *Dynamics of Heterogeneous Materials* (Springer-Verlag, New York, 2001).

[33] X. Jia, Th. Brunet, and J. Laurent, Phys. Rev. E **84**, 020301 (R) (2011).

[34] S. van den Wildenberg, M. van Hecke, and X. Jia, Europhys. Lett. **101**, 14004 (2013).

[35] J. R. Royer, B. Conyers, E. I. Corwin, P. J. Eng, and H. M. Jaeger, Europhys. Lett. **93**, 28008 (2011).

[36] S. T. Thoroddsen and A. Q. Shen, Phys. Fluids **13**, 4 (2001).

[37] G. Caballero, R. Bergmann, D. van der Meer, A. Prosperetti, and D. Lohse, Phys. Rev. Lett. **99**, 018001 (2007).

[38] J. R. Royer, E. I. Corwin, A. Flior, M.-L. Cordero, M. L. Rivers, P. J. Eng, and H. M. Jaeger, Nat. Phys. **1**, 164 (2005).

[39] X. Cheng, G. Varas, D. Citron, H. M. Jaeger, and S. R. Nagel, Phys. Rev. Lett. **99**, 188001 (2007).

[40] By substitution, one may verify that $P(x) = P^{*}\exp\{\exp[(\ln(\beta)/(\chi_2 - \chi_1))(x - c_1)]\}$ satisfies Eqs. (4)–(6), while also having the correct power law relation between P_{χ_1} and P_{χ_2}.

[41] S. R. Waitukaitis and H. M. Jaeger, Nature (London) **487**, 205 (2012).

[42] L. Labous, A. D. Rosato, and R. N. Dave, Phys. Rev. E **56**, 5717 (1997).

[43] N. V. Brilliantov, F. Spahn, J.-M. Hertzsch, and T Pöschel, Phys. Rev. E **53**, 5382 (1996).

[44] R. Ramirez, T. Pöschel, N. V. Brilliantov, and T. Schwager, Phys. Rev. E **60**, 4465 (1999).

[45] For $\varepsilon(P) \sim P^{\alpha}$, we find that $P(x) = [\alpha(c_1 + x)]^{-1/\alpha}$, and P_{χ_2} then asymptotes to a constant for large P_{χ_1}.